International Journal of Nanoelectronics and Materials
IJNeaM
ISSN 198-5761 | E-ISSN 2232-1535

Extraction of Bioactive Secondary Metabolites from *Citrus Maxima* Peel Via Pressurized Hot Water Extractor for the Synthesis of Iron Oxide Nanoparticles

Yi-Peng Teoh[a], Nurdalilah Othman[b,c], Sung-Ting Sam[b,c,d,*], Zhong-Xian Ooi[e], Wei-Wen Liu[d], Saparu Walli[f], Lian-See Tan[g], and Boon-Beng Lee[b]

[a]*Department of Petrochemical Engineering, Faculty of Engineering and Green Technology, Universiti Tunku Abdul Rahman, Jalan Universiti, Bandar Barat, 31900 Kampar, Perak, Malaysia.*
[b]*Faculty of Chemical Engineering & Technology, Universiti Malaysia Perlis (UniMAP), Kompleks Pusat Pengajian Jejawi 3, 02600 Arau, Perlis, Malaysia.*
[c]*Center of Excellence Geopolymer and Green Technology, Universiti Malaysia Perlis (UniMAP), 01000, P.O. Box 77, D/A Pejabat Pos Besar, Kangar, Perlis, Malaysia.*
[d]*Institute of Nano Electronic Engineering, Universiti Malaysia Perlis, Seriab, Kangar, Perlis, 01000, Malaysia.*
[e]*Department of Chemical Science, Faculty of Science, Universiti Tunku Abdul Rahman, Jalan Universiti, Bandar Barat, 31900 Kampar, Perak, Malaysia.*
[f]*Frutania Industry Sdn. Bhd., Lot 1 & 2, Kawasan Industri MARA Jejawi, Jalan Kangar-Arau 01000 Kangar, Perlis, Malaysia.*
[g]*Universiti Teknologi Malaysia, Department of Chemical Process Engineering, Malaysia – Japan International Institute of Technology, Jalan Sultan Yahya Petra, 54100 Kuala Lumpur, Malaysia.*
**Corresponding author. E-mail: stsam@unimap.edu.my*

ABSTRACT

Using bioactive secondary metabolites (BSM) from *Citrus maxima* peel extract, this work investigated a green method of synthesizing magnetite iron oxide (Fe_3O_4) nanoparticles (NPs). The BSM acts as a reducing cum stabilizing agent in the process. The optimization of the BSM parameters were conducted through response surface methodology (RSM). The optimal condition obtained in this study for pressurized hot water extractor (PHWE) extraction was temperature of 94.96 °C, solvent-to-solid ratio of 29.7 ml/g and extraction time of 27.6 min. BSM Yield of 49.31 % could be obtained based on this condition. The formation of Fe_3O_4 NPs were detected using the FTIR analysis with the absorption peaks observed at around 590 and 580 cm^{-1}. X-ray diffraction results matched standard magnetite Fe3O4 patterns with planes at (220), (311), (400), (511) and (440). Field emission scanning electron microscopy (FESEM) results showed that the magnetite Fe_3O_4 NPs synthesized in this study predominantly appeared in spherical shape. The extraction process's kinetics were examined using various empirical models, including the Elovich's model, Peleg's model, Power law and parabolic diffusion model. All applied models were found to be well fitted with the measured data from experiment, with R^2 values exceeding 0.9. Notably, the Peleg's model exhibited the highest R^2, the smallest RMSD, and the least significant p-values, indicating its superior performance.

Keywords: *Bioactive secondary metabolites, Extraction, Fruit peels, Magnetite iron oxide nanoparticles*

1. INTRODUCTION

Researchers have faith in nanotechnology with the rapid progression of technology and its potential to enhance the current quality of living [1]. Good superparamagnetic, biocompatibility, nontoxicity, high stability, and low cost of preparation of magnetite Fe_3O_4 NPs are the unique properties that have been considered as important factors in the synthesis of magnetite Fe_3O_4 NPs [2]. Magnetite Fe3O4 NPs can be contribute in various pharmaceutical applications [3], including electronics [4], [5], energy [6], biomedicine [7] and biotechnology [8].

The synthesis of magnetic NPs is one of the significant technique towards their application in biomedical and electronic applications [10]. Synthesis of magnetite Fe_3O_4 NPs could be conducted via hydrothermal synthesis, thermal decomposition, co-precipitation, and sol-gel methods [11]. Co-precipitation is deemed to be the best synthesis method as the particles obtained was found to be of controlled particle size [12], good homogeneity, high purity of product, required low cost, and without the need of organic solvents [13]. Currently, green production of NPs from plant extracts, mainly crop residues, are under development. For the sake of safeguarding the environment, green nanotechnology could eliminate or at least minimize the use of toxic substances. Most researchers successfully synthesized magnetite Fe_3O_4 NPs using green tea. The green synthesis method of producing nanoparticles is more environmentally friendly, safer and less toxic . However, limited studies were reported on the synthesis of magnetite Fe_3O_4 NPs from agro-industrial residues, particularly using pomelo peels.

Pomelo *Citrus maxima*, also known as *Citrus grandis* (L.) Osbeck, is a type of tropical fruits that exist naturally in Southeast Asia [14]. Malaysian commonly called that type of pamelo as limau bali, limau jambua, limau besar, limau betawi, limau bol, limau abong or Bali lemon. Based on data from Food and Agricultural Statistics, *C.maxima* is one of the top 5 Malaysia tropical fruits yields recorded in year 2018 . The yield for *C.maxima* was expected to rise for

upcoming years [15]. The peel of *C.maxima* pamelo is found to contain high bioactive secondary metabolites (BSM) [14] and reducing agent [16]. *C.maxima* pulp are normally considered as waste. In addition, pomelo waste generated from industries can occupy between 49 and 69 % of the initial fruit weight [17], [18]. Moreover, plants rich in antioxidants and polyols generally consist of hydroxyl and carboxyl groups. These groups could function as reducing and stabilizing agents. These agents could facilitate the NPs synthesis. Meanwhile, the phenolics and alkaloids may function as capping and stabilizing agents for reduced NPs [19]. Furthermore, the stable bond between phytochemicals in the extract and metallic NPs yielded the stability of NPs. Rahman et al.[20] reported the peel part of pomelo possesses the highest antioxidant assays, which mainly focus on the ferric reducing ability potential (FRAP). BSMcan be extracted using traditional or modern extraction techniques.

Conventional approach for bioactive compounds extractions such as solid-liquid extraction (SLE), liquid-liquid extraction (LLE), Soxhlet extraction, and maceration are time-consuming, of low extraction efficiency, and needs to utilize large amounts of toxic organic solvents in the process [21]. In recent years, pressurized hot water extraction (PHWE) has gained traction for isolating bioactive compounds from plants as well as food materials. The benefits of PHWE includes simplifying the extraction process, reducing the solvent use and improving the extraction rate [22]. Generally, phenolic compounds' most optimum extraction conditions were found between 80ºC – 150ºC and extraction duration (or time) of 1 to 60 min [23]. Plaza and Turner found that the best yield for extraction of antioxidant compounds using PHWE was achieved at 120 °C with extraction time of 3 minutes [24]. In another example, the authors compared the extraction reported the extraction yield of BSM from *Citrus unshiu* peel was the highest when using PHWE in comparison to extraction using hot water, methanol and ethanol [25]. Pressure, solvent-to-solid ratio, extraction time and temperature are the factors that could influence the extraction efficiency of PHWE [21], [26]. Therefore, PHWE attracted considerable attention due to its reduction of solvent consumption, temperature selectivity, high efficiency, environmentally friendly, and low cost in comparison to classical methods [21].

However, there is a limited reported study on the optimization, simulation, and modelling of PHWE process. In fact, the application of mathematical modelling could facilitate optimization, simulation, design and process control. Consequently, optimized process parameters, such as temperature, time and amount of solvent used, could be obtained. Meanwhile, the kinetics of PHWE process for extraction of plant roots has been previously assessed [27]. However, the extraction kinetic study for BSM using PHWE extractor have yet to be investigated.

On the other hand, there is limited reported study on the process parameter optimization for BSM of *C. maxima* extraction using PHWE and no data also reported on the green synthesis of magnetite Fe_3O_4 NPs using *C. maxima* as a reducing agent under optimized condition. So far, there is no kinetic study results available in open literature on the Power law, Peleg's, Parabolic and Elovich models on the BSM extraction using PHWE. Hence, as part of our effort, we investigated the optimal conditions for the operational factors, specifically the extraction time, solvent-to-solid ratio in PHWE and extraction temperature, for maximizing the BSM yield. It was followed by the synthesis of magnetite Fe_3O_4 NPs using the optimized *C. maxima* peel extracts. This method provides us a facile green synthesis route. It is also beneficial to utilize agriculture waste rather than burning it, which could pollute the environment.

2. MATERIALS AND METHODS

2.1. Chemicals

N-hexane, sodium hydroxide ferric chloride hexahydrate, ferrous chloride tetrahydrate were purchased from Bendosen, Malaysia.

2.2. Plant Materials

Citrus maxima peels were collected from food stalls at Padang Besar, Perlis, Malaysia. For removing of the dirt, the samples were washed using distilled water. Then, the samples were dried in at 50 ºC an oven, overnight. The samples were ground and sieved to 125 µm for standardized size. Next, using n-hexane and at room temperature, the samples were defatted (based on solid-to-liquid ratio of 1:10 (w/v)) followed by solvent evaporation. The defatted pomelo was peeled off for drying in the oven for 6 hours at 40 ºC.

2.3. Extraction of Bioactive Secondary Metabolites (BSM)

The pressurized hot water extraction (PHWE) was performed. One gram of defatted *C.maxima* was put into a 50 ml stainless steel extraction cell. Other parameters, namely solvent to solid ratio, extraction temperature and extraction duration (or time), were optimized. Distilled water was used for all the extractions. Obtained extracts were allowed to cool at ambient temperature. thereafter, filter paper (Whatman No 1) was used to separate the supernatant. Using a rotary evaporator, the supernatant was concentrated. The percentage yield of crude BSM extract was determined using Equation 1. All extractions were performed triplicates to evaluate the reproducibility of the PHWE results.

$$Percentage\ yield\ (\%) = \frac{(mass\ of\ crude - mass\ of\ flask\ (g))}{mass\ of\ sample\ (g)} x100\% \quad (1)$$

2.4. One-Factor-at-a-time Experimental Design (OFAT)

The preliminary Box-Behnken design (BBD) range was investigated by conducting one factor at-a-time (OFAT) series of experiment to identify independent variables, including extraction temperatures from 30 to 150 ºC, extraction time from 5 to 55 minutes and the ratio of solvent-to-solid from 20 to 50 (ml/g). The crude BSM yield

was designated as the response variable. For each experiment, two variables remained constant and only one variable was adjusted at a time. Each experiment was replicated three times to ensure the consistency and reliability of the results.

2.5. Design of Experiment (Box-Behnken Design)

The former one-factor at-a-time experiments were the basic results. To optimize the extraction conditions of BSM, Box Behken Design coupled with RSM was applied. Table 1 shows three parameters, i.e. X_1 is the extraction temperature, while X_2 and X_3 are the extraction time, and solvent-to-solid ratio. The factors of the process are coded as shown in Equation 2 for the statistical calculation.

$$x_i = X_i - X_0/\Delta X \quad i = 1,2,3 \tag{2}$$

Here, x_i and X_i represent the parameter's coded value and the actual parameter value. X_0 is the actual value of X_i at the central point, and ΔX represents the increment value. Using Design Expert 6.0.6 software, the collected data were subjected to analysis of variance (ANOVA) to optimize the three selected parameters temperature (A,°C), time (B, min) and solvent to solid ratio (C, g/ml) to improve the yield of extraction of crude BSM (%). The data from literature and preliminary OFAT experiments were used as basic results for determining the three independent factors at three levels (−1, 0, +1). Table 1 displays the experimental design in the current study. Total of 17-run of BBD consisted of completing the design.

Table 1 Parameters (temperatures (ºC), extraction time (min), solvent to solid ratio (ml/g)) and their levels

Parameters	Symbols	Levels		
		-1	0	+1
Temperatures (ºC)	X_1	60	90	120
Time (min)	X_2	15	25	35
Solvent to solid ratio (ml/g)	X_3	25:1	30:1	35:1

The extraction yield of unrefined BSM was modeled using a second-order polynomial equation. In order to establish an empirical model associated with the examined variables, a multiple regression analysis was conducted. The equation, as shown in Equation 3, was the employed second-order polynomial equation.

$$Y = \beta_0 + \sum_{i=1}^{3} \beta_i X_i + \sum_{i=1}^{3} \beta_{ii} X_i^2 + \sum_{i=1}^{2} \sum_{j=i+1}^{3} \beta_{ii} X_i X_j \tag{3}$$

Y is the predicted response for crude BSM extraction yield; β_0, β_i; β_{ii} and β_{ij} are the intercept, linear, quadratic and interaction effects' regression coefficients; X_i and X_j are the independent variables (i ≠ j). Based on the effect of the independent factors level, three-dimensional plots were obtained. These visual representations enabled the study of simultaneous interactions among the three independent factors on the yield response. By investigating these main factors, the optimum conditions were identified in the overlay plot.

2.6. Verification of the Model

The yield of the crude BSM depends on compositions of various media as obtained using RSM. In order to verify the model, the experiment was conducted on five separate occasions, and the outcomes of each trial were then compared to the expected values.

2.7. Green Synthesis of Magnetite Fe_3O_4 NPs

In the work, the method of green synthesis of Fe_3O_4 NPs was modified from the previous study [28]. About 60 mL of deionized water was bubbled with Nitrogen gas for 20 minutes and pressure of 1 bar. After that, 0.1988 g of $FeCl_2.4H_2O$ and 0.3244 g $FeCl_3.6H_2O$ (in 1:2 molar ratio) were dissolved in the solution. Then, the solution was rapidly stirred (700 rpm) with continuous bubbling of nitrogen gas for 20 minutes. The condenser was covered with parafilm and the solution was heated to 70˚C. Once the temperature target of 70˚C was achieved, 3 ml of plant extract was added to the solution. After 5 minutes, the solution was mixed with 5 mL of 2.5 Molar NaOH. The reaction was stirred for another 30 minutes. Thereafter, a permanent magnet was used to collect the black precipitate. The Fe_3O_4 NPs were collected by decanting after the temperature of the mixture was reduced to ambient temperature. Next, the sample was further diluted with deionized water for centrifugation. It was centrifuged at 10,000 rpm for 10 minutes. The Fe_3O_4 NPs were dried overnight at 80 ºC to be collected as powder form for characterization of Fourier Transform Infrared (FTIR), Field Emission Scanning Electron Microscope (FESEM) and X-Ray Diffraction (XRD) analysis. The chemical equation and biosynthesis flow process of the magnetite Fe_3O_4 NPs extracted from *C. maxima* were shown in Equation 4 and Figure 1.

$$Fe^{2+} + 2Fe^{3+} \xrightarrow{BSM} Fe_3O_4 + 4H_2O \tag{4}$$

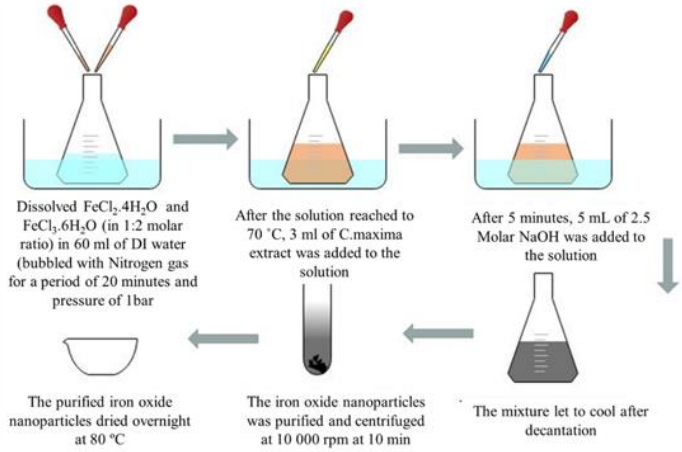

Figure 1. Flow process of the extraction protocol of magnetite Fe_3O_4 NPs from *C. maxima*.

2.8. Characterization of Magnetite Fe_3O_4 NPs

Magnetite Fe_3O_4 NPs were examined by FT-IR spectrophotometer (Spectrum Two-Perkin Elmer Model) at ambient temperature using KBr pellets method with ratio 1:100 w/w in the range 4000-400 cm^{-1}. For X-ray diffractometer, a setting of 30 kV/30mA, using Ni as filter was applied for Shimadzu model XRD-6000, which used CuKα as its radiation source. D-spacing was computed using Bragg's law, as shown in Equation 5. All XRD data were obtained within the angular range of $10º \leq 2\,\Theta \leq 80º$ under the specified experimental conditions. For the analysis of synthesized magnetite NPs, a Field Emission Scanning Electron Microscopy (FESEM) machine, specifically the Hitachi S-4500 model. To prepare thin films of magnetite NPs, a small quantity of the sample was applied onto a gold-coated copper grid. Excess solution was cleaned using blotting paper. Finally, the film was dried for 5 minutes under a mercury lamp.

$$\lambda = 2d \sin\theta \tag{5}$$

2.9. Selected Empirical Models on the Extraction Kinetic

In the current study, 4 two-parametric kinetic models were used, and the recovered solutes for modelling were validated by assuming that the fruit peel was isotropic and the size is equal, the distribution of extraction yield in the fruit peel was even and primarily dependent on the passage of time. Net diffusion occurred solely toward the outer surface of the fruit peel, a constant diffusion coefficient of extraction yield.

2.10. Parabolic Diffusion Model

Generally, the use of the parabolic diffusion equation was implemented to determine the process governed by diffusion [29]. Plecas (2003) effectively characterized waste radioactive composites using this particular model [30]. This model can be correlated using Equation 6, y is the extraction yield, Ai represents the parameter that needs to be established, and t represents the extraction time (in unit of minutes). This empirical equation pertains to a two-step extraction process, encompassing washing and diffusion stages, without any involvement of chemical reactions [31]. Subsequently, Equation 6 can be transformed into Equation 7, with A_0 and A_1 representing the washing coefficient and the constant for diffusion rate, respectively.

$$y = \sum_{i=0}^{n} A_i t^{1/2} \tag{6}$$

$$y = A_0 + A_1 t^{1/2} \tag{7}$$

2.11. Power Law Model

The power law model has been widely applied in the active agent diffusion process through non-swelling devices [32]. The model is related in Equation 8, in which y is the extraction yield, in this context, B represents the constant that encapsulates the interaction between the active agent and the carrier. The t and n indicates the time (minutes) and the exponent that characterizes the diffusion process, respectively. The n should be lesser than 1 (N < 1) for plant material extraction [33]. The determination of the parameters for this model was accomplished through a regression analysis. The linearized relationship is illustrated in Equation 9.

$$y = Bt^n \tag{8}$$

$$\ln(y) = nln(t) + \ln(B) \tag{9}$$

2.12. Peleg's Model

Peleg's model is a mathematical model commonly used to represent the extraction profile of biocompounds [34], [35]. In our current study, BSM extraction from *Citrus maxima* peel was adapted into the model as can be seen in Equation 10.

$$y = y_0 + \frac{t}{K_1 + K_2 t} \tag{10}$$

Where y_0 denotes the initial product yield at the beginning of the extraction when time is equals to zero , t is the time measured in minutes over which the extraction occurs, while K_1 and K_2 are the constants corresponding to the Peleg's rate and the Peleg's capacity. Equation 11 is the simplified form of Equation 10, with the assumption that the target product was not present at the start of the extraction process (at $t = 0$).

$$y = \frac{t}{K_1 + K_2 t} \tag{11}$$

2.13. Elovich's Model

Elovich's model can be used to study the correlation between the adsorption rate and the extraction yield. The model is expressed as in Equation 12 [36].

$$y = E_0 + E_1 \ln(t) \tag{12}$$

2.14. Model Validation

The models was simulated using experimental data and their evaluation involved the utilization of the root mean square deviation (RMSD) and the linear correlation coefficient (R_2) [26]. RMSD was calculated using Equation 13. Meanwhile, Equation 14 was used to calculate the value of mean relative percentage deviation, P. Y_{exp} and Y_{calc} are experimental and predicted BSM extraction yield and Fe3O4 NPs yield, respectively, whereas N is the number of data. According to Paterson et al. [37], a model can be accepted when the P values are below 10%.

$$RMSD = \sqrt{\frac{1}{N}\sum_{i=1}^{N}\left(y_{exp} - y_{calc}\right)^2} \quad (13)$$

$$p\ value = \frac{100}{n} x \sum \frac{\left|y_{exp} - y_{calc}\right|}{y_{exp}} \quad (14)$$

3. RESULTS AND DISCUSSION

3.1. Screening of the Range of Independent Factors Using OFAT data

OFAT was a helpful method especially in the determination of RSM levels although these single variable methods are overlooked in the interaction between different factors and are tedious to execute. As noted earlier, this OFAT presented three different factors: temperature, extraction times and solvent-to-solid ratio. Thus, the optimal levels of the factors can increase the production of crude BSM.

3.2. Effect of Extraction Temperature

Temperature of extraction was previously found as the most important parameter which affected the efficiency of extraction [25]. With a suitable temperature, targeted BSM undergo physical adsorption in the sample matrices and release chemical compounds into extraction solvents [38]. Chemical properties of solvent could be modified by reducing the concentration and raising the diffusion, thus resulting in a significant contribution of the mass transportation to the target compounds. Figure 2a shows the temperature effect (30, 60, 90, 120 and 150 ºC) on the crude BSM yield while the remaining parameters, i.e. solvent-to-solid ratio was set at 30 ml/g and extraction time was set at 25 min. As observed from the graph, when the temperature increased from 30 to 90 ºC, the BSM yield increased. At 90°C, the BSM yield was maximum at 50.63 ± 2.18 %. By increasing the extraction temperature, the crude BSM yield decreased slightly, indicating that the thermal degradation of BSM may lead by excessive temperature [39]. Therefore, 90 ºC was applied in the subsequent extraction experiments as optimum extraction temperature.

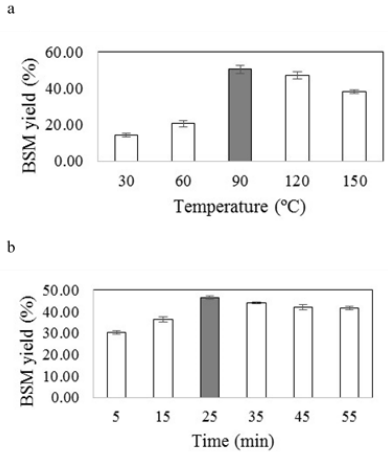

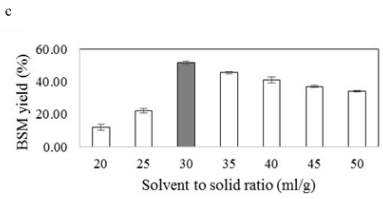

Figure 2. The effect of (a) temperature, (b) extraction time, and (c) solvent to solid ratio on the extraction yield of BSM. The experimental conditions were (a) 30 ml/g of solvent to solid ratio and 25 min of extraction time; (b) 30 ml/g of solvent to solid ratio and 90 ºC of temperature; (c) 90 ºC of temperature and 25 min of extraction time.

3.3. Effect of Extraction Time

The rate of extraction and quality of the extracted compounds could be influenced by extraction time [40]. Since the solvent needs time to permeate, dissolve and form materials to diffuse out, the extraction time is a crucial parameter to get better extraction yield. Based on the environmental perspective, reducing the energy required and cost of production are among the main concerns of researchers in the extraction process. Figure 2b shows the impact of increasing extraction time to the BSM extraction yield. It can be observed that in the first 25 min, the BSM yield increased with an increased extraction time, resulting in 46.63 ± 0.88 %. Thereafter, the crude BSM yield decreased gradually. This could be to the accelerating chemical decomposition of the compound during the extraction process. The higher temperature with long extraction time results in reduced extraction yield, especially under conditions of pressurized hot water [41]. In addition, the lowest extraction yield for this extraction was at 55 minutes with 41.65 ± 0.95 % and supported by [42], the extraction longer than 60 min was expected to be less significant. Therefore, 25 min of the extraction time was set in the subsequent extraction experiments.

3.4. Effect of Extraction Solvent-to-Solid

In PHWE extraction, the solvent-to-solid ratio is acknowledged as a crucial factor that influences extraction efficiency. This is because the ratio depends on the analytes distribution in water [40]. Various solvent-to-solid ratios can affect the concentrations of the exterior solvent and the interior plant cells. Hence, the yield of the extracted BSM could be significantly impacted by this factor. As presented in Figure 2c, the extraction yield of BSM initially increased with the increase of solvent-to-solid ratio. The maximum yield obtained in this study was 51.75 ± 1.10 % when the solvent-to-solid ratio was 30 ml/g. The yield tended to decrease thereafter, even as the solvent-to-solid ratio was increased. The reason is that while a specific solvent-to-solid ratio could increase the diffusion rate of the solvent into the cells, beyond that, it also enhanced the leaching-out rates of BSM [43]. However, an excess of solvent could cause cavitation of energy from the extraction system to be consumed. Hence, it could result in a lower crude BSM due to the more complicated the extraction procedure. Hence, electricity

and costing of time could be minimized by using 30 ml/g of a solvent-to-solid ratio.

3.5. Optimization of Process Parameters for RSM Extract Crude Yield using RSM

From OFAT methods, three independent factors (temperature, time and solvent-to-solid ratio) were used to determine the optimum levels. In the current study, a correlation between the three independent factors were developed by the application of BBD, with the aim of achieving higher extraction yield of *Citrus maxima*. The actual value of the experiment design and its coded version are tabulated in Table 2.

Table 2 The BSM yield (%) of the optimization parameters (temperatures (ºC), extraction time (min), solvent to solid ratio (ml/g)) using BBD

Run	Independent factors			Extraction yield (%)
	A (Temperature, ºC)	B (Extraction times, min)	C (Solvent to solid ratio, ml/g)	
1	90 (0)	35 (+1)	35 (+1)	43.91 ± 1.21
2	90 (0)	15 (-1)	25 (-1)	43.00 ± 0.15
3	60 (-1)	15 (-1)	30 (0)	31.94 ± 1.64
4	60 (-1)	25 (0)	25 (-1)	32.51 ± 0.74
5	90 (0)	25 (0)	30 (0)	48.71 ± 0.72
6	120 (+1)	35 (+1)	30 (0)	40.89 ± 0.64
7	90 (0)	25 (0)	30 (0)	49.40 ± 2.84
8	90 (0)	25 (0)	30 (0)	48.28 ± 0.62
9	90 (0)	25 (0)	30 (0)	49.48 ± 2.90
10	120 (+1)	25 (0)	35 (+1)	38.08 ± 1.70
11	90 (0)	35 (+1)	25 (-1)	43.82 ± 0.17
12	60 (-1)	35 (+1)	30 (0)	35.89 ± 2.05
13	90 (0)	25 (0)	30 (0)	48.37 ± 0.93
14	90 (0)	15 (-1)	35 (+1)	39.73 ± 1.36
15	120 (+1)	15 (-1)	30 (0)	40.48 ± 0.72
16	120 (+1)	25 (0)	25 (-1)	38.55 ± 0.68
17	60 (-1)	25 (0)	35 (+1)	30.03 ± 0.53

The predicted response *Y* (crude BSM yield) was obtained in terms of coded values as shown in Equation 3 through ANOVA using Design Expert 6.0.6 software. Each factor is represented by one coefficient of that factor itself. Meanwhile, those with second-order coefficients represented quadratic effects of the two interaction factors, respectively. Synergistic and antagonistic effects are shown by positive and negative signs in front of the terms. For the response surface of the quadratic model, F-test and the ANOVA confirmed the statistical significance of Equation 15, which are summarized in Table 3.

$$Y_{yield} = 48.85 + 3.45A + 1.17B - 0.77C - 0.89AB + 0.50AC + 0.84BC - 9.69A^2 - 1.86B^2 - 4.37C^2 \quad (15)$$

The p-value served as a metric to assess the significance of each coefficient in the model; a lower p-value indicates a more significant coefficient. Table 3 shows the ANOVA analysis results of the proposed regressed quadratic model. The results coefficients with exceptionally low probability values (P > F) below 0.0001 are significant, as determined by the F-test. Additionally, R^2 (0.9979) proposed that 99.79% for BSM yield trend could be explained using the selected independent factors. The desired adequate precision, which is used to assess the signal-to-noise ratio is deemed satisfactory if it exceeds 4. With a ratio of 55.345, the polynomial quadratic model is deemed to provide a strong signal, indicating its suitability for guiding exploration within the design space.

Table 3 Analysis of Variances (ANOVA) of BSM Yield Produced by *C. maxima*

Source	Sum of Squares	Degree of Freedom	Mean Square	F value	(P) > F
Model	643.15	9	71.46	365.16	< 0.0001
A	95.43	1	95.43	487.62	< 0.0001
B	10.95	1	10.95	55.96	0.0001
C	4.70	1	4.70	24.00	0.0018
A^2	3.13	1	3.13	16.01	0.0052
B^2	1.01	1	1.01	5.16	0.0573
C^2	2.82	1	2.82	14.42	0.0067
AB	394.96	1	394.96	2018.21	<0.0001
AC	14.61	1	14.61	74.65	<0.0001
BC	80.42	1	80.42	410.92	<0.0001
Residual	1.37	7	0.20		
Lack of fit	0.096	3	0.032	0.10	0.9558
Pure error	1.27	4	0.32		
Cor Total	644.52	16			

A response over a region's desired factor level, the interaction between the response and experimental levels of each factor showed the interaction types of the factors deduced (maximum, minimum and saddle points of

response) shown through a three-dimensional surface plot [44]. Figure 3a – c are a three-dimensional surface plot of BSM yield obtained based on the impact of temperature, time and solvent-to-solid ratio. The three-dimensional plot (Figure 3(a)) indicates that the yield had significantly increased with the increase of temperature, up to about 90 ºC, then decreased gradually and achieved a maximum yield at about 49.48 %. A similar trend was observed in Figure 3b and Figure 3c.

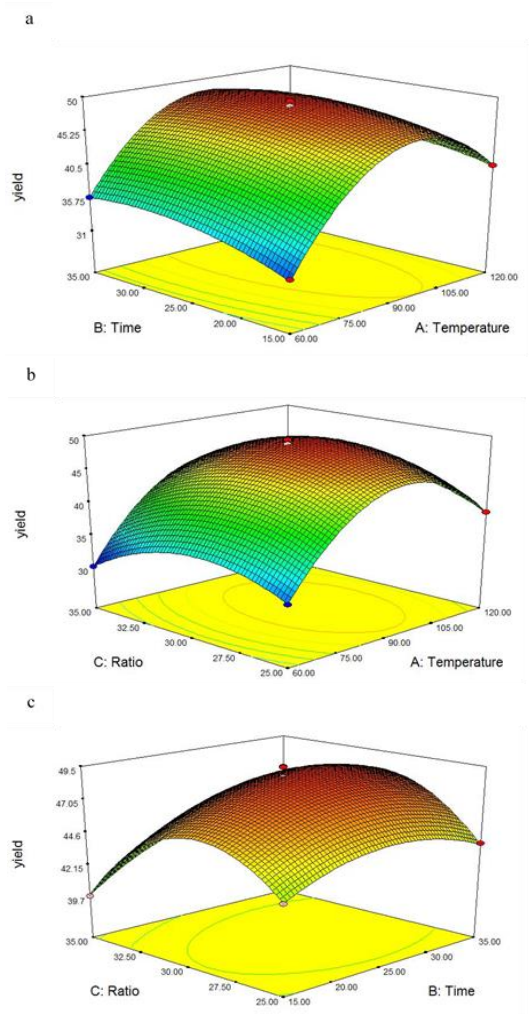

Figure 3 A three-dimensional visualization of the interactions between (a) temperature and time. Solvent-to-solid ratio was set at 30 ml/g. (b) temperature and solvent-to-solid ratio. Extraction time was set at 25 min. (c) extraction time and solvent-to-solid ratio. Extraction temperature was set at 90 ºC.

The interaction between solvent-to-solid ratio, temperature and time, and its impact towards the BSM yield was also visualized through the three-dimensional plot. Based on the analysis, the optimum condition to achieve maximum BSM yield was 94.96 ºC, 27.6 min and 29.7 ml/g solvent to solid ratio. It is predicted that 49.31 % of BSM yield could be obtained. The value of desirability was 0.991 (~1.00), which supports the model of the used application. The optimum temperature, mainly for phenolic compound, was reported to range from 80 – 150 ºC [40]. For the extraction time, the optimum extraction time was 27.6 min, and most of the BSM was recovered within the first 30 minutes [45]. Due to this condition, the optimum time obtained at higher temperatures suggested that the extraction time was acceptable. Other than that, for the solvent-to-solid ratio, there was a slight difference between the optimum ratio and the reported data, which is 25 ml/g [40]. The differing of obtained outcome of BSM extraction may be due to a slightly higher temperature applied and different types of samples. However, the solvent-to-solid ratio is close to the literature value, suggesting that the optimum ratio obtained was acceptable.

3.6. Characterization of Magnetite Fe_3O_4 NPs

Randomly, five sets of trials were repeated to confirm the model adequacy by obtaining a maximum yield of crude BSM. The absolute errors of percentage differences between the values from experimental results and predicted results ranged from 0.041 to 0.487 %. The validity of the model was verified since the differences were always less than 1%. For optimization, this model is suitable for BSM extraction using PHWE since they have a good correlation between experimental and predicted values which possessed the model of regression was accurate and adequate.

3.7. Characterization of Magnetite Fe_3O_4 NPs

The optimum conditions of BSM were used to synthesize magnetite Fe_3O_4 NPs. Three characterizations: FTIR, XRD and FESEM were conducted. The FTIR spectrum of the magnetite Fe_3O_4 NPs is shown in Figure 4. The presence of Fe_3O_4 NPs is indicated by three distinct absorption bands linked to the Fe-O stretching vibration in bulk magnetite, i.e. 630, 585 and 433 cm^{-1}. The peak seen at 1062 cm^{-1} is due to the C-N stretching vibrations from aliphatic amines [45]. In the FTIR spectrum of *Citrus maxima* powder, there is a specific stretching vibration band ranging from 1377 – 1248 cm^{-1}, which is representative of polysaccharide group. This band disappeared after the formation of Fe_3O_4 NPs, suggesting that polysaccharide group are involved in the reduction and stabilization of Fe_3O_4 NPs. This findings aligns with findings by Yuvakkumar and Hong [46], which noted that polysaccharides had a good ability to synthesize nanoparticles. Furthermore, the peak at 1637 cm^{-1} indicated the conjugated carbonyl (C=O) group stretching vibration. Interaction f a C=O group with the nanoparticles contributed to the band shift from 1637 cm^{-1} to 1555 cm^{-1}[47]. In addition, the peak at 1751 cm^{-1} corresponds to the C=O bond stretching (carboxylic group), which also disappeared after Fe_3O_4 NPs synthesis, denoted the phytochemicals present in the plant extract [48], [49].

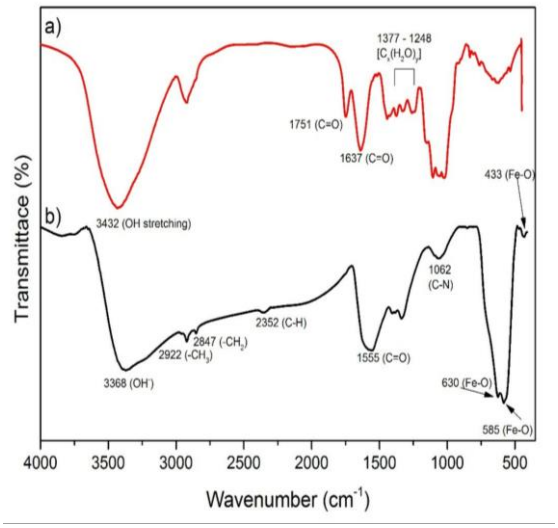

Figure 4. a) Fourier Transform Infrared (FTIR) of *C. maxima* extract and b) Fourier Transform Infrared (FTIR) of magnetite Fe_3O_4 NPs.

Hydroxyl signals were also observed at 3432 cm^{-1} (OH bond stretching) and 3368 cm^{-1} (OH^-). The decrease of intensity at 3432 cm^{-1} after reduction of $FeCl_3$ indicated the inclusion of the OH groups from water molecules and phenolic compounds in the reduction process, resulting in overlapped peaks at 3368 cm^{-1} [50]. The stabilizing, reducing and capping agents role in the synthesis of nanoparticles was contributed from hydroxyl and carboxylic groups [20]. Absorption band at 2922 cm^{-1} and 2847 cm^{-1} indicates C-H stretch in methyl ($–CH_3$) and methylene ($–CH_2$) aliphatic saturated (C–H) sharp asymmetric and symmetric stretching [50]. Peak 2352 cm^{-1} is related to C-H stretching [51]. The *C. maxima* extract used for green synthesis of magnetite iron oxide were found to contain BSM like polyphenols. The polyphenols reduced Fe^{2+}/Fe^{3+} to nanozerovalent iron or iron nanoparticles. From FTIR spectroscopy, the polyphenols contained in *C. maxima* extract may be assumed to have the ability to act as reducing, capping and stabilizer for magnetite nanoparticles.

The typical XRD pattern of the magnetite NPs is shown in Figure 5. The diffraction peaks of the Fe_3O_4 NPs were similar to those reported in the Joint Committee on Powder Diffraction Standards (JCPDS) data cards (87-2334). Several peaks were noticed at 30.2° (220), 35.5° (311), 43.0° (400), 57.2° (511) and 62.9° (440). The peaks existed in agreement with Yew and other researchers [52]. A good crystalline structure was indicated by the presence of sharp and narrow peaks of magnetite Fe_3O_4 NPs have.

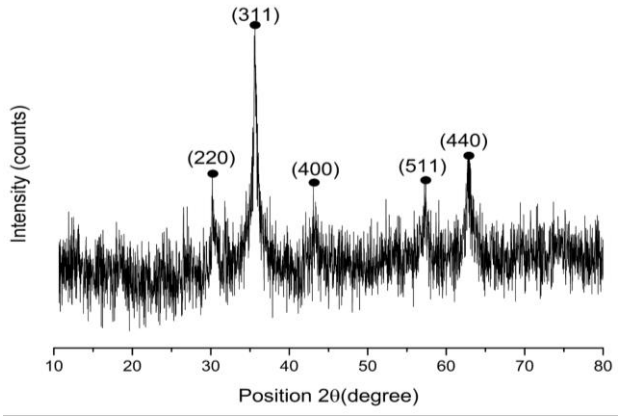

Figure 5. XRD patterns of magnetite Fe_3O_4 NPs synthesized with addition of *C. maxima* extracts.

The morphology of the magnetite Fe_3O_4 NPs in comparison with *C. maxima* peels are observed in FESEM images and presented in Figure 6a and Figure 6b. *C. maxima* peels The peels are mainly composed of cellulose-based structural proteins. Hence, they are of fibrous content and with insoluble cell walls. As shown in Figure 5a, the *C. maxima* peels has more fibre and active sites. These green synthesis of magnetite Fe_3O_4 NPs appear in spherical shape shown in Figure 6b. The size, on average, was found to be 9.09 nm. Excellent internalization rate and high cellular uptake was exhibited by spherical NPs, instead of nanodisk, nanocube or nanorods (another shape). Some of the agglomerates were seen due to strong inter-particles van der Waals and magnetic interaction. There were few irregular shapes observed as well, may be due to the agglomeration process. Using a co-precipitation method, the size of magnetite NPs would range from 5 to 100 nm [53], [54]. This range of size makes the NPs suitable in biomedical field since those are comparable to the sizes of a gene (which is approximately 10 to 100 nm long and 2 nm wide), a protein (which is within the range of 5 to 50 nm) and a virus (which is within the range of 20 to 500 nm) [55].

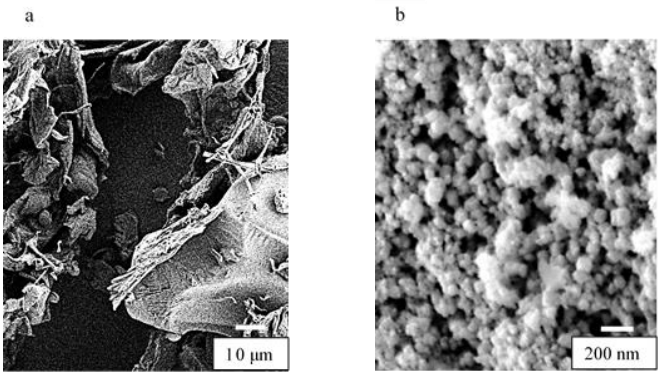

Figure 6. FESEM images of a) parent *C. maxima* peel and b) the magnetite iron oxide NPs synthesized with addition of *C. maxima* extract.

3.8. Kinetic Modelling

There are two stages of extraction kinetic models. The initial phase is a rapid washing action, while the later stage is a slower diffusion-controlled extraction. During the process, there is rapid extraction of easily accessible extractive substances, and it was rather difficult to monitor the washing stage [32]. Figure 7 (a) shows the extraction yield versus time profile for the *C. maxima* extract that was produced under the optimized extraction temperature (94.96%) and solvent-to-solid ratio (29.7 ml/g), respectively. The yield of BSM was 49.31 %, as mentioned in section 3.2. Fe_3O_4 NPs profile (Figure 7(b)) also showed a similar trend as Figure 7(a). In this study, four empirical kinetic models were chosen to fit the experimental data from the extraction curves. The kinetic models include the Elovich's model, parabolic diffusion model, Peleg's model and Power law model.

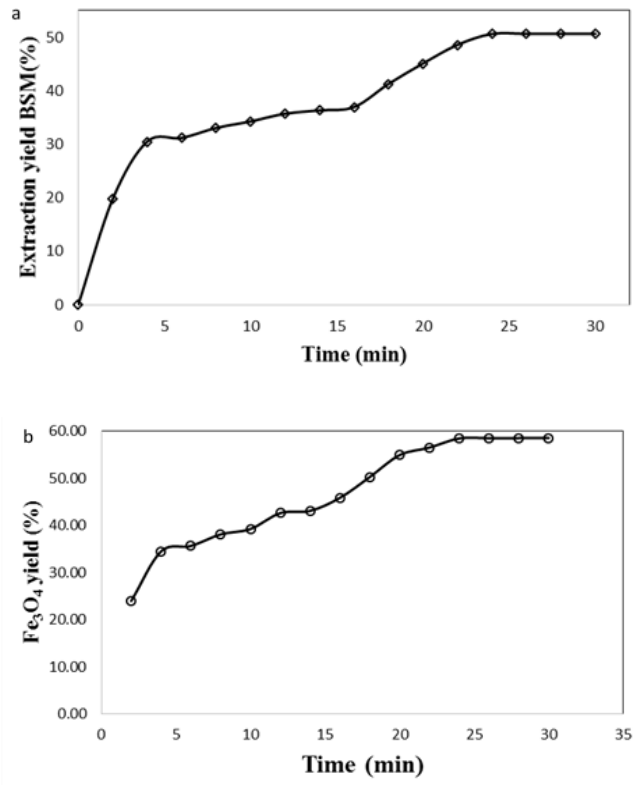

Figure 7. Extraction profile for (a) extraction yield and (b) Fe_3O_4 NPs from *Citrus maxima* extract under the optimized condition 94.96 °C and 29.7 ml/g.

Table 4 summarizes the chosen empirical kinetic models and its linearized form. In this study, the BSM extraction yield and the Fe_3O_4 NPs yield from the experiments were analysed using the kinetic model's linearized form.

Table 4 Selected kinetic models and its linearized equation

Models	Equation	Linearized equation
Parabolic diffusion model	$y = A_0 + A_1 t^{1/2}$	-
Power law model	$y = Bt^n$	$\ln(y) = n\ln(t) + \ln(B)$
Peleg's model	$y = y_0 + \frac{t}{K_1 + K_2 t}$	$y = \frac{t}{K_1 + K_2 t}$
Elovich model	$y = E_0 + E_1 \ln(t)$	-

The computed parameters for the chosen empirical models are outlined in Table 5. The statistical values are also listed in the table. Notably, in the case of the parabolic diffusion model, the A_0, which represents washing coefficient for Fe_3O_4 NPs yield production exceeded the extraction yield. The results indicated a higher solubility of the Fe_3O_4 NPs yield in the 29.71 ml/g solvent-to-solid ratio at the initial time (when time was equal to zero). The rate of diffusion (A_1) during the extraction process was 7.3802 %/$min^{0.5}$, whereas the diffusion rate for Fe_3O_4 NPs was 13.5430 7.3802 %/$min^{0.5}$. This showed that Fe_3O_4 NPs performed higher diffusion coefficients in the extraction. For Power law and Elovich's model, the kinetic parameters also showed a similar trend. It can be observed that the BSM yield showed a lower diffusion rate as compared to Fe_3O_4 NPs yield. Conversely, in Peleg's model, the K_1 value corresponds to the extraction rate while K_2 indicates the concentration at equilibrium condition. As shown in Table 5, the BSM yield extraction revealed a higher value of K_1 (=0.1075 min/%) and K_2 (=0.0165 1/%) compared to the yield of Fe_3O_4 NPs. According to Karacabey et al. [36], the higher values of extraction rate and concentration at equilibrium condition indicated acceleration of the substances extracted. Consequently, a higher equilibrium concentration was achieved.

Table 5 Model parameters and statistical values correlated

Model parameters	Statistical values	Extraction yield	
		BSM yield	Fe_3O_4 yield
Parabolic diffusion model			
A_0 (%)		11.5250	13.5430
A_1 (%/$min^{0.5}$)		7.3802	8.6675
	R^2	0.9412	0.9641
	RMSD	2.2140	2.0100
	P value (10^{-9})	2.2200	0.0900
Power law model			
n		0.3264	0.3274
B (1/min^n)		16.7350	19.6210

	R^2	0.9353	0.9623
	RMSD	0.0650	0.0490
	P value (10^{-9})	4.1700	0.1230
Peleg's model			
K_1 (min/%)		0.1075	0.0888
K_2 (1/%)		0.0165	0.0142
	R^2	0.9565	0.9713
	RMSD	0.0300	0.0210
	P value (10^{-9})	0.3140	0.0206
Elovich model			
E_0 (%)		10.3880	12.0650
E_1 (%/min)		11.4750	13.5320
	R^2	0.9004	0.9299
	RMSD	2.8820	2.8060
	P value (10^{-9})	69.800	7.0200

Figure 8 shows the predicted and experimental data profile for the BSM extraction from *C. maxima* peel under the optimized condition of solvent-to-solid ratio of 29.7 ml/g and 94.96 °C using the selected extraction kinetic models. The R^2 values exceeded 0.9, indicating that the predicted results could closely model the actual condition's results. Based on the results, the R^2 values ranged between $0.9009 < R^2 < 0.9713$ for all the tested models. Hence, it can be deduced that the two-stage process of fast-washing action and slow-diffusion in the BSM extraction process and the yield of Fe_3O_4 NPs were decently captured by the selected empirical models. On the other hand, the comparison of different empirical models involved the use RMSD which represents the root mean square deviation to further verify the appropriateness of the models. According to Kitanović et al. [33], a better model fit reflected a higher R^2 value and lower RMSD value. In the current findings, the RMSD value ranged from 0.0210 to 2.8820, indicating A strong concordance between the observed and simulated data.

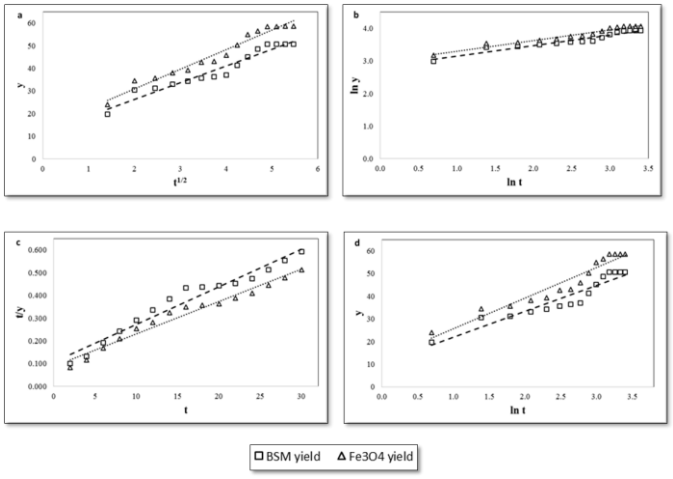

Figure 8. Experimental and predicted results at optimum condition for the BSM yield and Fe_3O_4 yield. Experimental data is represented by the square and triangle symbols while the predicted data is in line form (a) Parabolic diffusion model, (b) Power law model, (c) Peleg's model, and (d) Elovich's model.

P values the empirical kinetic model were determined for further assessing the best fitting models to predict the BSM extraction and Fe_3O_4 NPs yields. If the P value is below 10%, the model is considered acceptable [37]. Based on the summarized data (Table 5), each one of the selected models was adequate in expressing the kinetic behaviour of BSM extraction and Fe_3O_4 NPs yields. It was noticed that the P values ranged between 0.0206 - 69.8000 (10^{-9}). In comparison, Peleg's model showed the highest R^2 value, the lowest RMSD value, and the smallest P value in both BSM extraction yield and Fe_3O_4 NPs yield. Therefore, Peleg's model was chosen as the best empirical model for expressing BSM extraction and Fe_3O_4 NPs yield from *C. maxima* peel.

CONCLUSION

The green approach applied this study to synthesize magnetite Fe_3O_4 NPs, using *Citrus maxima* extract without chemical-based reducing agent and stabilizer, was successfully conducted. Polyphenols compounds may be assumed to act as reducing and stabilizing agents greener in the synthesize process. The optimum synthesis parameters of *C. maxima* extract using PHWE were obtained at 94.96 °C, 27.6 min and 29.7 ml/g of solvent-to-solid ratio. Then, the optimized condition of plant extract was used to synthesize magnetite Fe_3O_4 NPs using co-precipitation method successfully. The FTIR result showed the presence of polyphenols and other BSM in the extract of peel *C. maxima*, which verified the successful synthesis of magnetite Fe_3O_4 NPs with the appearance of absorption peaks at the range of 590 cm^{-1} and 580 cm^{-1}. For XRD analysis, crystal peaks of magnetite Fe_3O_4 NPs were seen. In addition, FESEM images showed a mostly spherical shape of magnetite Fe_3O_4 NPs with an average size 9.09 nm were synthesized. In this study, Peleg's model was found to be the best suited kinetic model for BSM extraction and Fe_3O_4 NPs yield production from *C. maxima* peel. The green synthesized magnetite Fe_3O_4 NPs are expected to have

wide applications, especially in biomedical, healthcare, environment, agriculture and construction.

ACKNOWLEDGMENTS

The authors would like to acknowledge the financial support from the UniPRIMA grant (9001-00670) funded by Universiti Malaysia Perlis. This work has also been supported by the Fundamental Research Grant Scheme (FRGS) under a grant number of FRGS/1/2015/TK02/UNIMAP/02/05 from the Ministry of Education Malaysia.

REFERENCES

[1] S. Priest, "The North American opinion climate for nanotechnology and its products: Opportunities and challenges," *J. Nanoparticle Res.*, vol. 8, no. 5, pp. 563–568, 2006, doi: 10.1007/s11051-005-9060-7.

[2] N. F. Attia *et al.*, "Applied Surface Science Advances Iron oxide nanoparticles and their pharmaceutical applications," *Appl. Surf. Sci. Adv.*, vol. 11, no. April, p. 100284, 2022, doi: 10.1016/j.apsadv.2022.100284.

[3] M. Yusefi, K. Shameli, R. R. Ali, S. Pang, and S. Teow, "Evaluating Anticancer Activity of Plant-Mediated Synthesized Iron Oxide Nanoparticles Using Punica Granatum Fruit Peel Extract," *J. Mol. Struct.*, p. 127539, 2020, doi: 10.1016/j.molstruc.2019.127539.

[4] S. Fang, D. Bresser, and S. Passerini, "Transition Metal Oxide Anodes for Electrochemical Energy Storage in Lithium- and Sodium-Ion Batteries," vol. 1902485, 2019, doi: 10.1002/aenm.201902485.

[5] A. K. Singh, "Nanostructured coatings based on metallic nanoparticles as viral entry inhibitor to combat COVID-19," *Sustain. Mater. Technol.*, vol. 35, no. September 2022, p. e00544, 2023, doi: 10.1016/j.susmat.2022.e00544.

[6] K. Tuharin, M. Zan, P. Kudrna, and M. Tich, "Iron Oxide and Iron Sulfide Films Prepared for Dye-Sensitized Solar Cells," 2020.

[7] R. G. D. Andrade, S. R. S. Veloso, and E. M. S. Castanheira, "Shape Anisotropic Iron Oxide-Based Magnetic Nanoparticles : Synthesis and Biomedical Applications," 2020.

[8] V. Magdanz, J. Gebauer, P. Sharan, S. Eltoukhy, D. Voigt, and J. Simmchen, "Sperm – Particle Interactions and Their Prospects for Charge Mapping," vol. 1900061, pp. 1–9, 2019, doi: 10.1002/adbi.201900061.

[9] A. Ali *et al.*, "Synthesis, characterization, applications, and challenges of iron oxide nanoparticles," *Nanotechnol. Sci. Appl.*, vol. 9, pp. 49–67, 2016, doi: 10.2147/NSA.S99986.

[10] F. S. Hasany, I. Ahmed, J. Rajan, and A. Rehman, "Systematic Review of the Preparation Techniques of Iron Oxide Magnetic Nanoparticles," *Nanosci. Nanotechnol.*, vol. 2, no. 6, pp. 148–158, 2013, doi: 10.5923/j.nn.20120206.01.

[11] W. Wu, Z. Wu, T. Yu, C. Jiang, and W.-S. Kim, "Recent progress on magnetic iron oxide nanoparticles: synthesis, surface functional strategies and biomedical applications," *Sci. Technol. Adv. Mater.*, vol. 16, no. 2, p. 023501, 2015, doi: 10.1088/1468-6996/16/2/023501.

[12] Z. Cheng *et al.*, "Synthesis and Characterization of Iron Oxide Nanoparticles and Applications in the Removal of Heavy Metals from Industrial Wastewater," vol. 2012, 2012, doi: 10.1155/2012/608298.

[13] M. Nazari, N. Ghasemi, and H. Maddah, "Synthesis and characterization of maghemite nanopowders by chemical precipitation method," pp. 2–6, 2014, doi: 10.1007/s40097-014-0099-9.

[14] P. Vijaylakshmi and R. Radha, "An overview: Citrus maxima," *J. Phytopharm. JPHYTO*, vol. 4, no. 45, pp. 263–267, 2015.

[15] D. Qu, "Fruit production in Malaysia," *Food and Agriculture Organization of the United Nations*, 2020. [Online]. Available: http://www.fao.org/faostat/en/#home.

[16] N. N. Prabhu, "Green synthesis of iron oxide nanoparticles (IONPs) and their nanotechnological applications," *J. Bacteriol. Mycol. Open Access*, vol. 6, no. 4, pp. 260–262, 2018, doi: 10.15406/jbmoa.2018.06.00215.

[17] S. Vijayalaxmi, S. K. Jayalakshmi, and K. Sreeramulu, "Polyphenols from different agricultural residues: extraction, identification and their antioxidant properties," *J. Food Sci. Technol.*, vol. 52, no. May, pp. 1–9, 2014, doi: 10.1007/s13197-014-1295-9.

[18] D. Yun and J. Liu, "Recent advances on the development of food packaging films based on citrus processing wastes: A review," *J. Agric. Food Res.*, vol. 9, no. March, p. 100316, 2022, doi: 10.1016/j.jafr.2022.100316.

[19] J. J. Toh, H. E. Khoo, and A. Azrina, "Comparison of antioxidant properties of pomelo [Citrus Grandis (L) Osbeck] varieties," *Int. Food Res. J.*, vol. 20, no. 4, pp. 1661–1668, 2013.

[20] N. F. A. Rahman, R. Shamsudin, A. Ismail, and N. N. A. Karim Shah, "Effects of post-drying methods on pomelo fruit peels," *Food Sci. Biotechnol.*, vol. 25, pp. 85–90, 2016, doi: 10.1007/s10068-016-0102-y.

[21] N. A. N. Mohamad, N. A. Arham, J. Jai, and A. Hadi, "Plant Extract as Reducing Agent in Synthesis of Metallic Nanoparticles: A Review," *Adv. Mater. Res.*, vol. 832, no. November, pp. 350–355, 2013, doi: 10.4028/www.scientific.net/AMR.832.350.

[22] C. C. Teo, S. N. Tan, J. W. H. Yong, C. S. Hew, and E. S. Ong, "Pressurized hot water extraction (PHWE)," *J. Chromatogr. A*, vol. 1217, no. 16, pp. 2484–2494, 2010, doi: 10.1016/j.chroma.2009.12.050.

[23] Y. Tian, Y. Wang, Y. Ma, P. Zhu, J. He, and J. Lei, "Optimization of subcriticalwater extraction of resveratrol from grape seeds by response surface methodology," *Appl. Sci.*, vol. 7, no. 4, pp. 1–12, 2017, doi: 10.3390/app7040321.

[24] M. Plaza and C. Turner, "Pressurized hot water extraction of bioactives," *TrAC - Trends Anal. Chem.*, vol. 71, pp. 39–54, 2015, doi: 10.1016/j.trac.2015.02.022.

[25] M. Plaza, V. Abrahamsson, and C. Turner, "Extraction and neoformation of antioxidant compounds by

pressurized hot water extraction from apple byproducts," *J. Agric. Food Chem.*, vol. 61, no. 23, pp. 5500–5510, 2013, doi: 10.1021/jf400584f.

[26] S. Q. Chang and A. Azrina, "Antioxidant content and activity in different parts of pomelo [Citrus grandis (L.) Osbeck] by-products," pp. 27–34, 2017, doi: 10.17660/ActaHortic.2017.1152.4.

[27] C. Cheigh, E. Chung, and M. Chung, "Enhanced extraction of flavanones hesperidin and narirutin from Citrus unshiu peel using subcritical water," *J. Food Eng.*, vol. 110, no. 3, pp. 472–477, 2012, doi: 10.1016/j.jfoodeng.2011.12.019.

[28] N. Rahimi, M. Shiva, S. A. Mortazavi, A. H. Elhamirad, A. M. Maskooki, and G. Rajabzadeh, "Kinetic study of superheated water extraction of berberine from Berberis vulgaris root," *Bulg. Chem. Commun.*, vol. 47, no. Special issue D, pp. 140–146, 2015.

[29] A. H. M. Yusoff, M. N. Salimi, and M. F. Jamlos, "Synthesis and Characterization of Biocompatible Fe3O4 Nanoparticles at Different pH," vol. 020010, pp. 1–5, 2017, doi: 10.1063/1.4981832.

[30] A. Bucic-Kojic, M. Planinic, M. Bilic, and D. Velic, "Study of solid – liquid extraction kinetics of total polyphenols from grape seeds," *Food Eng.*, vol. 81, pp. 236–242, 2007, doi: 10.1016/j.jfoodeng.2006.10.027.

[31] I. B. Plecas, "Comparison of mathematical interpretation in radioactive waste leaching studies," vol. 258, no. 2, pp. 435–437, 2003.

[32] J. Youl, C. Lak, and C. Hyun, "Modeling of nuclide release from low-level radioactive paraffin waste : a comparison of simulated and real waste," vol. 94, pp. 161–178, 2002.

[33] S. Kitanovic, D. Milenovi, and V. B. Veljkovic, "Empirical kinetic models for the resinoid extraction from aerial parts of St . John ' s wort (Hypericum perforatum L .)," *Biochem. Eng. J.*, vol. 41, pp. 1–11, 2008, doi: 10.1016/j.bej.2008.02.010.

[34] A. Sturzoiu, M. Stroescu, A. S. Guzun, and T. Dobre, "Empirical Models Applied for Kinetics Extraction of β -carotene from Rosa canina," *REV.CHIM.(Bucharest)*, no. 3, pp. 3–7, 2011.

[35] M. Peleg, "An empirical model for the description moisture sorption curves," *J. Food Sci.*, vol. 53, no. 4, pp. 1216–1217, 1988.

[36] E. Karacabey, L. Bayindirli, N. Artik, and G. Mazza, "Modeling solid-liquid extraction kinetics of trans-resveratrol and trans-e-viniferin from grape cane," *J. Food Process Eng.*, 2011, doi: 10.1111/j.1745-4530.2011.00660.x.

[37] I. F. Paterson, B. Z. Chowdhry, and S. A. Leharne, "Polycylic aromatic hydrocarbon extraction from a coal tar-contaminated soil using aqueous solution of nonionic surfactants," *Chemosphere*, vol. 38, no. 13, pp. 3095–3107, 1999.

[38] F. Kaymak-ertekin and A. Gedik, "Sorption isotherms and isosteric heat of sorption for grapes , apricots , apples and potatoes," *Leb. u.-Technol*, vol. 37, pp. 429–438, 2004, doi: 10.1016/j.lwt.2003.10.012.

[39] R. ElGamal, C. Song, A. M. Rayan, C. Liu, S. Al-Rejaie, and G. ElMasry, "Thermal Degradation of Bioactive Compounds during Drying Process of Horticultural and Agronomic Products: A Comprehensive Overview," *Agronomy*, vol. 13, no. 6, 2023, doi: 10.3390/agronomy13061580.

[40] T. Yajie, W. Yingsa, M. Yunyun, Z. Pengbo, H. Jing, and L. Jiandu, "Optimization of subcritical water extraction of resveratrol from grape seeds by response surface methodology," pp. 1–12, 2017, doi: 10.3390/app7040321.

[41] J. Liu, M. Sandahl, P. J. R. Sjöberg, and C. Turner, "Pressurised hot water extraction in continuous flow mode for thermolabile compounds: Extraction of polyphenols in red onions," *Anal. Bioanal. Chem.*, vol. 406, no. 2, pp. 441–445, 2014, doi: 10.1007/s00216-013-7370-7.

[42] X. Qi, X. Peng, Y. Huang, L. Li, and Z. Wei, "Green and efficient extraction of bioactive flavonoids from Equisetum palustre L . by deep eutectic solvents-based negative pressure cavitation method combined with macroporous resin enrichment," vol. 70, pp. 142–148, 2015, doi: 10.1016/j.indcrop.2015.03.026.

[43] C.-S. Seo, J.-H. Kim, and H.-K. Shin, "Optimization of the extraction process for the seven bioactive compounds in Yukmijihwang-tang, an herbal formula, using response surface methodology," *Pharmacogn. Mag.*, vol. 10, no. 39, p. 606, 2014, doi: 10.4103/0973-1296.139798.

[44] S. S. Kankara, M. Mustafa, H. M. Ibrahim, R. Nulit, and R. Go, "Effect of Drying Methods, Solid-Solvent Ratio, Extraction Time and Extraction Temperature on Phenolic Antioxidants and Antioxidant Activity of Guiera senegalensis J.F. Gmel (Combretaceae) Leaves Water Extract," *Am. J. Phytomedicine Clin. Ther.*, vol. 2, no. 12, pp. 1378–1392, 2014.

[45] Â. P. Matos *et al.*, "Optimization of biomass production of Chlorella vulgaris grown in desalination concentrate," 2014, doi: 10.1007/s10811-014-0451-y.

[46] R. Yuvakkumar and S. I. Hong, "Green Synthesis of Spinel Magnetite Iron Oxide Nanoparticles," *Adv. Mater. Res.*, vol. 1051, no. June, pp. 39–42, 2014, doi: 10.4028/www.scientific.net/AMR.1051.39.

[47] A. M. Awwad and N. M. Salem, "A Green and facile approach for synthesis of magnetite nanoparticles," *J. Mater. Environ. Sci.*, vol. 2, no. 3, pp. 285–292, 2011, doi: 10.5923/j.nn.20120206.09.

[48] D. Oosthuizen *et al.*, "Solvent Extraction of Polyphenolics from the Indigenous African Fruit Ximenia caffra and Characterization by LC-HRMS," *Antioxidants*, vol. 7, no. 8, p. 103, 2018, doi: 10.3390/antiox7080103.

[49] M. Mahdavi, F. Namvar, M. Bin Ahmad, and R. Mohamad, "Green biosynthesis and characterization of magnetic iron oxide (Fe3O4) nanoparticles using seaweed (Sargassum muticum) aqueous extract," *Molecules*, vol. 18, no. 5, pp. 5954–5964, 2013, doi: 10.3390/molecules18055954.

[50] R. R. R. Kannan, W. A. Stirk, and J. Van Staden, "Synthesis of silver nanoparticles using the seaweed Codium capitatum P.C. Silva (Chlorophyceae)," *South African J. Bot.*, vol. 86, pp. 1–4, 2013, doi: 10.1016/j.sajb.2013.01.003.

[51] M. Stan *et al.*, "Removal of antibiotics from aqueous solutions by green synthesized magnetite

nanoparticles with selected agro-waste extracts," *Process Saf. Environ. Prot.*, 2017, doi: 10.1016/j.psep.2017.03.003.

[52] Y. P. Yew *et al.*, "Green synthesis of magnetite (Fe3O4) nanoparticles using seaweed (Kappaphycus alvarezii) extract," *Nanoscale Res. Lett.*, vol. 11, no. 1, p. 276, 2016, doi: 10.1186/s11671-016-1498-2.

[53] H. Hasana and E. Desalegn, "Characterization and Quantification of Phenolic Compounds from Leaf of Agarista salicifolia," *Herb. Med. Open Access*, vol. 03, no. 01, pp. 1–5, 2017, doi: 10.21767/2472-0151.100022.

[54] N. Yousif, S. Al-Jawad, A. Taha, and H. Stamatis, "A review of Structure, Properties, and Chemical Synthesis of Magnetite Nanoparticles," *J. Appl. Sci. Nanotechnol.*, vol. 3, no. 2, pp. 18–31, 2023, doi: 10.53293/jasn.2022.5179.1178.

[55] S. Trifunschi, M. F. Munteanu, V. Agotici, S. Pintea, and R. Gligor, "Determination of Flavonoid and Polyphenol Compounds in Viscum Album and Allium Sativum Extracts," *Int. Curr. Pharm. J.*, vol. 4, no. 5, pp. 382–385, 2015, doi: 10.3329/icpj.v4i5.22861.